Transient seepage during Class-V Underground Injection Control Well Borehole Infiltration Tests in Vashon Advance Outwash, Puget Lowland, Washington

Matthew J. Porter

A report prepared in partial fulfillment of

the requirements for the degree of

Master of Science

Earth and Space Sciences: Applied Geosciences

University of Washington

November 2017

Project mentors:
Curtis J. Koger, AESI
Jenny Saltonstall, AESI
Luke Mioduszewski, AESI

Internship coordinator:
Kathy Goetz Troost

Reading committee:
J. Michael Brown
Kathy Goetz Troost
Curtis J. Koger, AESI
Jenny Saltonstall, AESI
Luke Mioduszewski, AESI

MESSAGe Technical Report Number: 058

EXECUTIVE SUMMARY

The radius of influence and height of groundwater mounding of Class-V Underground Injection Control (UIC) well infiltration within Quaternary Vashon Advance Outwash (Q_{va}) is investigated and implications for regional regulation and design are considered. Class-V UIC wells for stormwater management infiltrate treated stormwater at depth beneath the land surface. The model method and sensitivity analysis outlined in this study can be used as part of well interference and down gradient impact assessment evaluating the adequacy of proposed infiltration facility design and the potential impacts to slope stability located within the zone of influence of the infiltration system.

Transient seepage flow above the water table for an axisymmetric layered model with a far field constant head boundary using site-specific conditions such as the stratigraphy, location of water table, and grain size is modeled with finite-element (FE) SEEP/W. The saturated hydraulic conductivity (K_{sat}) in the model (K_{model}) is calibrated to quasi-steady state stepped-flow rate infiltration tests. FE results are then used as ground truth to judge the adequacy of borehole permeameter (BP) solutions, six of which are reviewed for analytical estimation of K_{sat} ($K_{analytical}$). Finally, a sensitivity analysis exposes which parameters control the radius of influence and K_{model}. The radius of influence herein is defined as the radius of the bulb of saturation surrounding the well, and the length of mound measured where the mound decays 90% from the maximum amplitude in the x-direction from the well.

BP solutions make numerous assumption to translate infiltration rate into saturated hydraulic conductivity of the vadose zone. A combination of the Zhang (1998) and Reynolds (2010) solutions best match isotropic K_{model}. A major assumption in BP solutions is isotropic soil, yet, the Reynolds (1983) solution accurately predicts K_{model} under a vertical anisotropy ratio (K_h: K_v) of 10:1. Overall, these solutions match model results with approximately ±10% mean error.

Based on a sensitivity analysis, the most dominant material property affecting the radius of influence is the vertical anisotropy of hydraulic conductivity. This vertical anisotropy present in the Q_{va} is controlled by the degree of stratification. Increasing the vertical anisotropy decreases mound height and increases the radius of influence. This result agrees with analysis by Sumner et al. (1999) and disagrees with that by Carleton (2010) on groundwater mounding beneath infiltration basins. Increasing the vertical anisotropy from isotopic to 10:1 is accompanied by an average increase of 30% in K_{model}. Changing the volumetric water content curve to represent finer textures gives a small increase in the amplitude of the mound and radius of influence. Decreasing the effective porosity significantly reduced the time required for the mound to reach a quasi-steady state condition. These parameters dictate the shape and extent of the saturation bulb surrounding the UIC well and the mounding of the water table beneath.

The results have implications for current impact assessment and guidance on UIC design from Washington State Department of Ecology. First, certain BP methods can be used for in-situ determination of K_{sat} from borehole infiltration tests, streamlining the modeling process for impact assessments. The sensitivity of the groundwater mound amplitude and radius of influence to model variables suggest UIC wells under certain site conditions are less likely to meet requirements for treatment capacity and separation from the groundwater table. Finally, both unsaturated flow and a vertical anisotropy of 10:1 should be considered in future assessments of slope stability within the zone of influence of infiltration.

This project was supported by Associated Earth Sciences Inc. (AESI) in Kirkland, Washington.

ABBREVIATIONS

AESI: Associated Earth Sciences Inc.
BMP: Best management practice
BP: Borehole Permeameter
CAD: Computer aided drawing
GPM: Gallons per minute
GSI: Green Stormwater Infrastructure
GUI: Graphic User Interface
$K_{analytical}$: The saturated hydraulic conductivity as calculated from borehole permeameter solutions
K_{GS}: Saturated hydraulic conductivity calculated from grain size data
K_{model}: The saturated hydraulic conductivity as calibrated in the model
K_{sat}: Saturated hydraulic conductivity, estimated by $K_{analytical}$ and K_{model}
LID: Low Impact Development
MAE: Mean absolute error
ME: Mean error
MK: Modified Kovács
NRMSE: Normalized root mean square error
Q_{ob}: Olympia Non-glacial deposits
Q_{va}: Vashon Stade Advance Outwash
Q_{vlc}: Vashon Stade Lawton Clay
Q_{vt}: Vashon Stade Till
RMSE: Root mean square error
UIC: Underground Injection Control
USBR: United States Bureau of Reclamation
VWC: Volumetric Water Content curve. Also known as the water retention curve (WRC) or the saturated water characteristic curve (SWCC).
WAC: Washington Administrative Code
WRC: Water retention curve. Also known as the saturated water characteristic curve (SWCC) or volumetric water content curve (VWC).

MATHEMATICAL TERMS

$\boldsymbol{\alpha}$: Sorptive number or capillarity parameter
$\boldsymbol{C}$: Shape factor
$\boldsymbol{\gamma_w}$: Unit weight of water
$\boldsymbol{H}$: Total hydraulic head
K_h: Horizontal conductivity
K_v: Vertical conductivity
$\boldsymbol{m_w}$: Slope of the VWC storage curve
$\boldsymbol{n}$: Number of models run
$\boldsymbol{Q}$: Flux or flow rate
$\boldsymbol{r}$: Well radius
$\boldsymbol{u_w}$**:** Pore pressure
$\boldsymbol{y}$: Elevation head

CONTENTS

EXECUTIVE SUMMARY ..... **I**

ABBREVIATIONS ..... **II**

MATHEMATICAL TERMS ..... **II**

LIST OF FIGURES ..... **IV**

LIST OF TABLES ..... **IV**

INTRODUCTION **1**

Project Summary and Motivation 1
Scope of Work 1

BACKGROUND **2**

Regional Setting 2
Geologic and Hydrogeologic Setting 2
Quaternary Vashon Advance Outwash and Aquifer 3
Underground Injection Control (UIC) Wells 4
UIC Well Testing 4
Darcy's Law and Borehole Permeameter solutions 4

MODELLING IN SEEP/W **5**

Overview and Assumptions 5
Governing Equations 6
Material Properties 7
Borehole Boundary Conditions 9
Meshing 9

METHODS **10**

Calibration and Radius of Influence 10
Borehole Permeameter Solutions and Capillarity 10
Sensitivity Analysis 12

RESULTS **12**

Calibration 12
Comparison with Borehole Permeameter (BP) methods 12
Sensitivity Analysis 15

DISCUSSION AND CONCLUSIONS **17**

Future groundwater mounding analyses 17
Borehole permeameter solutions and the sorptive number 17
Impact on regional regulations and design 18

REFERENCES **19**

APPENDIX A: MODEL AND ANALYTICAL RESULTS **22**

APPENDIX B: BOREHOLE GEOMETRY, INFILTRATION TEST SUMMARY, AND GRAIN SIZE **24**

LIST OF FIGURES

Figure 1: Location of study sites in relation to Seattle, WA 2
Figure 2: Model overview with initial conditions, boundary conditions, and regions labeled. Exported from Geostudio software. 6
Figure 3: The volumetric water content curve in SEEP/W uses pore-water pressure (u_w) instead of $\boldsymbol{\Psi}$. From GEO-SLOPE International (2012) 7
Figure 4: Volumetric water content functions considered in this study. Curves that are hysteretic are labeled in the legend. 8
Figure 5: (A) Comparison of two unsaturated K functions in SEEP/W. (B) figure from Lebeau and Konrad (2010) showing components of capillary and adsorptive flow 9
Figure 6: Different boundary conditions as applied in each model type - (Left) Defining Head (Right) Defining Flux 9
Figure 7: Change in K from lower to higher head tests when the higher head test involved a larger portion of the screen [L]. 12
Figure 8: (above) Graph comparing K (feet/day) calculated in SEEP/W to BP methods at Kh/Kv = 1 and sorptive numbers specified in Table 2. (below) Graph comparing K (feet/day) calculated in SEEP/W to BP methods at Kh/Kv = 10 and sorptive numbers as specified in Table 2 13
Figure 9: Stephens (1979) equation sorptive numbers fitted each step individually to match isotropic K_{model}. Sorptive numbers decrease exponentially with head rise in tests where the head [H] is less than the length of the screen [L]. 14
Figure 10: Base case or control model for the sensitivity analysis. The bottom of the well is at 200 feet and the initial water table begins at 150 feet elevation. Isolines for the initial water table and after 1, 3, 5, and 20 days are marked. 15
Figure 11: Results of the sensitivity analysis: (A) Porosity decreased to 0.15; (B) porosity increased to 0.35; (C) VWC curve changed to silty sand; (D) VWC curve changed to gravel; (E) Isotropic medium; (F) Anisotropy increased to 100:1. 16

LIST OF TABLES

Table 1: Overview of borehole permeameter solution inputs and equations 11
Table 2: Summary of ME, MAE, and RMSE for $K_{analytical}$ relative to isotropic K_{model}. $^{1}\alpha=5m^{-1}$, $^{2}\alpha=2.1m^{-1}$, $^{3}\alpha=1.1m^{-1}$ 13
Table 3: ME, MAE, and RMSE for Reynolds (1983) $K_{analytical}$ to anisotropic K_{model} 13
Table 4: RMSE fitted sorptive number values from Stephen's (1979, 1987) and Reynolds (2010) solutions in comparison to value assumed in Weitering (2015) 14
Table 5: Capillarity descriptions modified from Reynolds and Elrick (1985) 14

INTRODUCTION

Project Summary and Motivation

Class-V underground injection control (UIC) wells are a practical and cost-effective technique to achieve Washington State Department of Ecology stormwater management goals to maximize infiltration from either new site development or redevelopment. UIC wells can be used to convey treated stormwater runoff into the subsurface through relatively impermeable deposits at the surface to an adequate infiltration receptor underneath. In the Puget Lowland, UIC wells typically infiltrate into the unsaturated portion of Vashon Stade advance outwash (Q_{va}) of the Fraser Glaciation. The Q_{va} is a glaciofluvial deposit composed of proglacial and glacially-derived sand and gravel, generally coarsening upwards, with localized zones of finer sand and silt (Troost and Booth, 2008). Low hydraulic conductivity beds that decrease vertical hydraulic conductivity are more commonly present in the lower section of the Q_{va}. Modeling provides an opportunity to assess the effects of Q_{va} anisotropy on the extent of groundwater mounding and the error of $K_{analytical}$ from borehole permeameter solutions relative to K_{model}.

SEEP/W, by GEO-SLOPE International Ltd., is a finite-element CAD software which can be used to simulate subsurface conditions during UIC well borehole infiltration tests using a transient unsaturated-saturated model with user-defined boundary conditions. The borehole infiltration tests studied in this paper include datalogger and flow rate measurements of 32 UIC wells across 4 sites in and around the Seattle area (Figure 1). SEEP/W has been previously used by AESI to assess off-site impacts of UIC wells to slope stability and groundwater mounding using steady-state models. Future infiltration studies could use this information as part of rigorous well interference and down gradient impact assessment of UIC wells that evaluate the adequacy of proposed infiltration facility design and the potential impacts to slope stability located within the zone of influence of the infiltration system.

This project was supported by Associated Earth Sciences Inc. (AESI) and builds off two prior MESSAGe studies completed by Mr. Lam Nguyen (2013) and Mr. Bart Weitering (2015) at AESI. Both studies focused on deriving hydraulic conductivity using grain-size data. Weitering (2015) considers borehole permeameter methods in his study, and in his conclusions, suggests that future studies should examine the capillarity parameter or sorptive number (α) of the Q_{va} and use numerical modeling to study the effects of scaling on borehole infiltration tests. AESI is a multi-disciplinary, professional geotechnical engineering, hydrogeological, geological, and environmental consulting firm with offices in Everett, Kirkland, and Tacoma, WA.

Scope of Work

Transient-state axisymmetric models are used in SEEP/W to simulate stepped-rate Class-V UIC well tests performed by AESI; using site conditions, a saturated hydraulic conductivity is calibrated (K_{model}) to match either the observed flow rate or water level. This K_{model} is equivalent to K_{sat}, the maximum hydraulic conductivity of the bulk Q_{va} material within the zone of influence of infiltration. Then, these values are compared to $K_{analytical}$ calculated from borehole permeameter methods (Zangar, 1953; Stephens, 1979; Reynolds et al., 1983; Stephens et al., 1987; Zhang et al., 1998; Reynolds, 2010). I assess which method(s) agree with K_{model} for future studies to use for prediction of K_{sat} within the model or as a simple estimation method independent of the model. I also investigate the sorptive number (α) by fitting it to the lowest RMSE in $K_{analytical}$ from Stephens (1979, 1987) or Reynolds (2010) and K_{model}. Flow in unsaturated conditions is influenced by several factors including but not limited to: the horizontal to

vertical hydraulic conductivity ratio (K_h:K_v) variations within the Q_{va}, the distance to the aquifer, the shape of the volumetric water content (VWC) function, and well development. I consider the sensitivity of the extent of the saturation bulb and groundwater mound to these model inputs of effective porosity, VWC functions, and K_h:K_v.

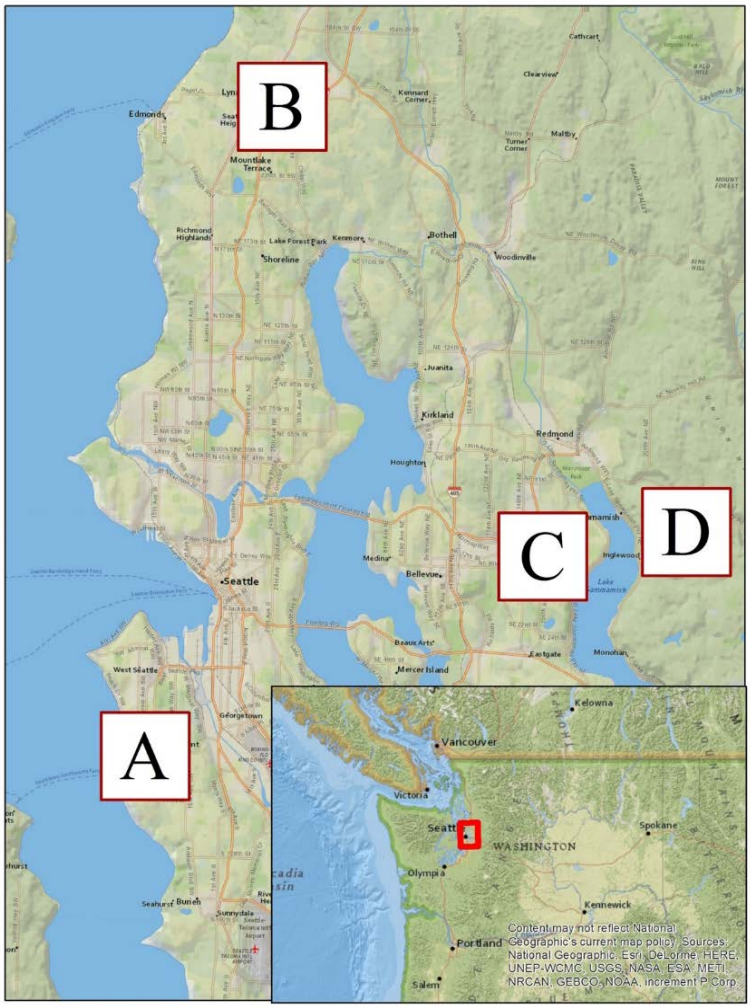

Figure 1: Location of study sites in relation to Seattle, WA

BACKGROUND

Regional Setting

The Puget Lowland is a structural and glacially-scoured basin bounded by the Cascade Range to the east and the Olympic Mountains to the west. The regional average rainfall is 43 inches per year (Joint Institute for the Study of the Atmosphere and Ocean, 2009). The Puget Lowland is well-developed, with a population of over 4 million, and its urban centers have significant percentages of impermeable surfaces that increase surface runoff and decrease aquifer recharge. During development or redevelopment, stormwater infiltration structures such as Class-V UIC wells are deployed to increase aquifer recharge. Q_{va} aquifer discharge is a source of cool, high-quality groundwater that maintains summer baseflow conditions. UIC wells also mitigate peak flows during winter storms by attenuating flows through aquifer storage and transit. Peak flows can damage aquatic habitats in rivers and streams and overload existing stormwater sewers. Low-impact development and green stormwater infrastructure initiatives are important in growing areas in and around Seattle where developments or redevelopments need to both conserve space and control stormwater runoff.

Geologic and Hydrogeologic Setting

The geology of the Puget Lowland is primarily composed of an alternating sequence of glacial and interglacial sediments that is both discontinuous and incomplete. Although the most recent glaciation ended 16-17 thousand calendar years ago, the Puget Lowland has been glaciated by segments of the Cordilleran Ice Sheet at least 7 times in the past 2.4 million years, all of which have advanced over Seattle (Porter and Swanson, 1998; Troost and Booth, 2008). The sequence creates an unconformity with the underlying and tectonically deformed bedrock, which is intermittently exposed at the surface.

The most recent glaciation of the Puget Lowland is the Vashon Stade of the Fraser Glaciation (Armstrong et al., 1965). Forming the southwestern extent of the Cordilleran Ice Sheet, the Puget Lobe advanced southward and dammed the Juan de Fuca Strait, depositing a progradational sequence of glaciomarine,

glaciolacustrine, and outwash in the Puget Lowland. The lowermost Fraser unit is the Lawton Clay member of the Vashon Stade (Q_{vlc}) which is composed of laminated clay and silt. As the Puget Lobe advanced further south, the depositional environment energy increased from glaciolacustrine to one with widespread deltaic and fluvial systems. The advance outwash of the Vashon Stade (Q_{va}) reflects these changes in a largely permeable and poorly-graded fine to medium sand that coarsens upwards to gravel and fines downwards near the transitional zone with the Q_{vlc} (where present). As the Puget Lobe advanced over regions within the Puget Lowland, paths of subglacial drainage carved deep erosional troughs which are later occupied by modern river systems and waterbodies such as Lake Washington and Puget Sound (Booth and Hallet, 1993). The Q_{va} deposits are discontinuous in these areas and where they abut high-relief paleotopography (Troost, 2016). The ice also scoured drumlins at the upland surface and deposited basal till of the Vashon Stade (Q_{vt}) discontinuously. Areas that were overridden have their underlying deposits glacially-consolidated, which rearranges, compresses, and dewaters sediments. As the Puget Lobe retreated, it deposited intermittent ice-contact material of sand and gravel while recessional outwash coalesced into channels and upland depressions. Modern deposits include river terraces (alluvium), landslides (colluvium), peat, and from human activity, fill. The Vashon Stade deposits are directly underlain by the Olympia interglacial deposits (Q_{ob}) or those from earlier glacial and interglacial periods.

As described by Vaccaro et al. (1998), the areal extent of the Fraser Glaciation drift delineates the Puget Sound aquifer system, particularly that of the Vashon Stade. The glacial and interglacial units can be divided into 3 hydrologic units: aquifers, semi-confining, and confining units. The aquifer units consist of coarse-grained units like proglacial, glaciofluvial and fluvial deposits. The fine-grained till, glaciomarine, glaciolacustrine and lacustrine units can be semi-confining or confining. Groundwater moves from topographic highs to topographic lows, the latter of which are stream drainages or salt water bodies (Vaccaro et al., 1998). The predominant flow direction is horizontal in the aquifer units and vertical in the confining and semi-confining units (Vaccaro et al., 1998).

Quaternary Vashon Advance Outwash and Aquifer

The Q_{va} is a glaciofluvial deposit composed of proglacial and glacial-derived sand and gravel, sometimes coarsening upwards. It forms an extensive and largely unconfined aquifer in the upper sequence of the Puget Lowland. The deposit is predominantly a permeable, uniform sand with trace amounts of fines (Troost and Booth, 2008), however, the lower transitional zone commonly contains interbeds of silt and clay while the upper zone is heterogeneous due to braided streams, point bars, and other fluvial structures. The unsaturated part of the Q_{va} has good potential for stormwater infiltration because of its adequate specific capacity and widespread thickness. Q_{va} is the most voluminous deposit in Seattle but its thickness varies across the Puget Lowland, ranging from tens to 400 feet thick (Galster and Laprade, 1991; Troost and Booth, 2008). The Q_{va} can be found at the surface or overlain by till, recessional outwash, ice-contact deposits, or fill, and underlain by Q_{vlc}, Q_{ob}, and other pre-Fraser deposits. Where the Q_{va} rests on less-permeable fine-grained material, groundwater exits laterally in the form of seeps and springs (Troost and Booth, 2008). The base elevation ranges from just below sea level to 900 feet above sea level (Turney et al., 1995).

Numerous sources detail the hydrologic properties of the Q_{va}. A prior AESI study by Nguyen (2013) provides a median of 6 feet per day for the field saturated hydraulic conductivity of over-consolidated sandy material (i.e. Q_{va}); Nguyen states this number is not purely vertical or horizontal conductivity. Other sources give a geometric mean of 33 to 35 feet per day for Q_{va} horizontal hydraulic conductivity (K_h) (Turney et al., 1995; Woodward et al., 1995); and average 2 feet per day for K_h in Q_{va} fine sand and

silt (Vaccaro et al., 1998). Current literature of the bulk vertical anisotropy of the Q_{va} aquifer give K_h:K_v ratios of 4:1 (DHI Water and Environment, 2009) to 10:1 (Morgan and Jones, 1996)

Underground Injection Control (UIC) Wells

The Washington Administrative Code (WAC) defines a UIC well as a man-made structure whose depth is deeper than its largest surface dimension with the purpose of discharging fluid into the subsurface via drain tiles, well screens, or similar mechanisms (State of Washington Department of Ecology Water Quality Program, 2006). Several Class-V UIC well designs exist. Two types of Class-V UIC wells that AESI has developed and refined include deep media-backfilled and water-well style. Media-backfilled wells are cased through the Q_{vt} (where present), left uncased in the Q_{va}, and backfilled with washed free-draining aggregate. The water-well style wells are cased through the Q_{vt} and not backfilled; instead, they are completed with steel mesh screens that extend at least 20 feet below the casing with a solid plate at the base. Water-well style Class-V UIC wells are then developed like water supply wells. The water-well style Class-V UIC wells are reviewed in this study. Media-backfilled style wells are not considered because of variables associated with the gravel-pack subsidence that occurs during testing and the potential for results hinged on the inputs of the material model and K_{model} of the washed aggregate, not the Q_{va}.

UIC Well Testing

AESI's protocol for UIC well borehole infiltration tests consists of increasingly stepped-flow rates that are each held constant for part of the approximately 8 consecutive hour test. The water level in the UIC well is allowed to reach near steady-state conditions before flow is increased. A step, as referred to in this study, includes a flow rate and its maximum associated head rise. At a minimum, a stepped-flow rate test would consist of two flow rates that are at and above the design rate. A maximum achievable flow rate is usually sustained for the last half of the test.

The flow rate and water level during the test are manually and digitally monitored. The flow rate is measured by an inline digital flow meter that displays instantaneous and total flow volumes. These volumes are recorded along with manual water-level measurements at regular (minute-scale) intervals, while a data logger submerged at the bottom of the well records the water level rise at short (second-scale) intervals. A barometer that is hung nearby records changes in air pressure for post-processing.

As previously noted by Weitering (2015), AESI's procedure does not conform to constant head borehole infiltration methods developed by the USBR. Their *Earth Manual Part II* states that head is considered constant when the change in head is less than two-tenths of a foot over a five-minute interval (U.S. Department of the Interior Bureau of Reclamation, 1990). AESI only includes steps that reach a steady-state condition in their respective geotechnical reports, therefore, only this data is used in the analysis. A French curve can be used to extrapolate remaining data until it meets this criterion, but was not performed in this study for replicability and because the practice has a small effect on calculations of conductivity (Weitering, 2015).

Darcy's Law and Borehole Permeameter solutions

Borehole permeameter (BP) solutions are equations that relate the rate of infiltration to the saturated hydraulic conductivity of the vadose zone. Their equations for $K_{analytical}$ use a variation of Darcy's Law that is parameterized for radial flow. In the mid-1800s, Henry Darcy experimentally derived the expression for the flow of water through porous media as the discharge (Q) is proportional to the gradient of the

total hydraulic head (i), the hydraulic conductivity (K), and cross-sectional area (A) (Fetter, 2001), such that:

$$Q = -KiA$$

Part of the parameterization includes solutions to the Laplacian equation in symmetric cylindrical coordinates. The Laplacian equation describes steady-state groundwater flow and its solutions derive a constant, called the shape factor (C), which is based on the geometry and the boundary conditions (Chapuis, 1998; Fetter, 2001). BP solutions use different shape factors, which are typically defined using the hydraulic head (H) and the well radius (r). Many shape factors are applied to the same general equation, as described by Elrick et al. (1989):

$$K = \frac{CQ}{[2\pi H^2 + C\pi r^2 + 2\pi H/\alpha]} \qquad \text{(Eq. 1)}$$

In the denominator, the components are the hydrostatic pressure flow, vertical gravity flow, and the capillary flow, respectively. The component of capillary flow depends on the sorptive number (α), which varies between soil textures and structures (Reynolds et al., 1983). The α-term is approximately equal to the inverse length of the capillary fringe, and thus in fine-grained soils with strong capillary effects α is small and coarse-grained soils with very weak or negligible capillary effects, α is large and approaches infinity. The above equation is further reduced with minor differences depending on the BP solution:

$$K_1 = \frac{CQ}{2\pi H^2} \qquad \text{(Eq. 2)} \qquad K_2 = \frac{CQ}{rH} \qquad \text{(Eq. 3)} \qquad K_3 = \frac{CQ}{2\pi L(H + {}^1/_{\alpha})} \qquad \text{(Eq. 4)}$$

Equation 2 only considers hydrostatic flow and is used in analytical solutions (Zangar, 1953; Reynolds et al., 1983). Zhang (1998) also uses this equation 2 but indirectly accounts for capillarity using a solution that is specific for sands. Equation 3 is unique to the Stephens (1979, 1987) regression equations because α is a component of the shape factor. Lastly, equation 4 is the single head radial flow equation from Reynolds (2010), where L is the screen length.

BP equations are applied within their original context along with key assumptions. The solutions have been conventionally used to calculate K_{sat} from the Guelph Permeameter or Air-Entry Permeameter in shallow, open boreholes. Until Reynolds (2010) shape factor equation, the screen interval was not incorporated into the equation. As such, all other equations are evaluated only for head levels that are less than the screen height. In addition, BP solutions have several key assumptions:

- Homogeneous and isotropic soil
- Soil is inert and does not shrink or swell
- Flow field is completely saturated
- Borehole development, smearing, and algae are non-issues
- Capillarity is neglected (Equation 2, except Zhang (1998))

MODELLING IN SEEP/W

Overview and Assumptions

Finite element analysis in SEEP/W has several advantages over other modeling approaches. One of the most significant advantages of SEEP/W over a program like MODFLOW is that it can perform

unsaturated analysis more readily. SEEP/W also can change the hydraulic anisotropy of materials rather than assuming they are isotropic or that anisotropy can be replicated using a multi-layer model in MODFLOW.

In SEEP/W, one has control over the three main parts in finite element analysis: drawing the geometry and discretizing the mesh, entering material properties, and specifying boundary conditions. The axisymmetric model in SEEP/W is ideal for calibration as it can simulate 3D by rotating the resulting 2D analysis about the x=0 axis. As a result, the flux through the screened length is calculated in 3D and thus is directly comparable to the flow rate into the well during testing. Axisymmetric models are typically used in SEEP/W for simulating flow into a single pumping well or flow out of a single recharge well into a uniform aquifer (GEO-SLOPE International, 2012).

The model makes assumptions about aquifer properties, initial conditions, and boundary conditions (Figure 2). First, the model represents the Q_{va} aquifer as one homogeneous layer and assumes that properties of the Q_{va} along the UIC well are indicative of the rest of the aquifer. Second, the initial water table is assumed to be flat. Third, a constant head boundary condition at far-field (several hundred feet) allows flux out of the model to maintain constant head. Fourth, a no-flow boundary is assumed at the base of the model. Fifth, all flow out of the well is assumed to be radial; an impermeable end plate is typically placed at the base of these wells and this is drawn in the model. Lastly, the model assumes that infiltration instrumentation is accurate and borehole development is a non-issue.

Figure 2: Model overview with initial conditions, boundary conditions, and regions labeled. Exported from Geostudio software.

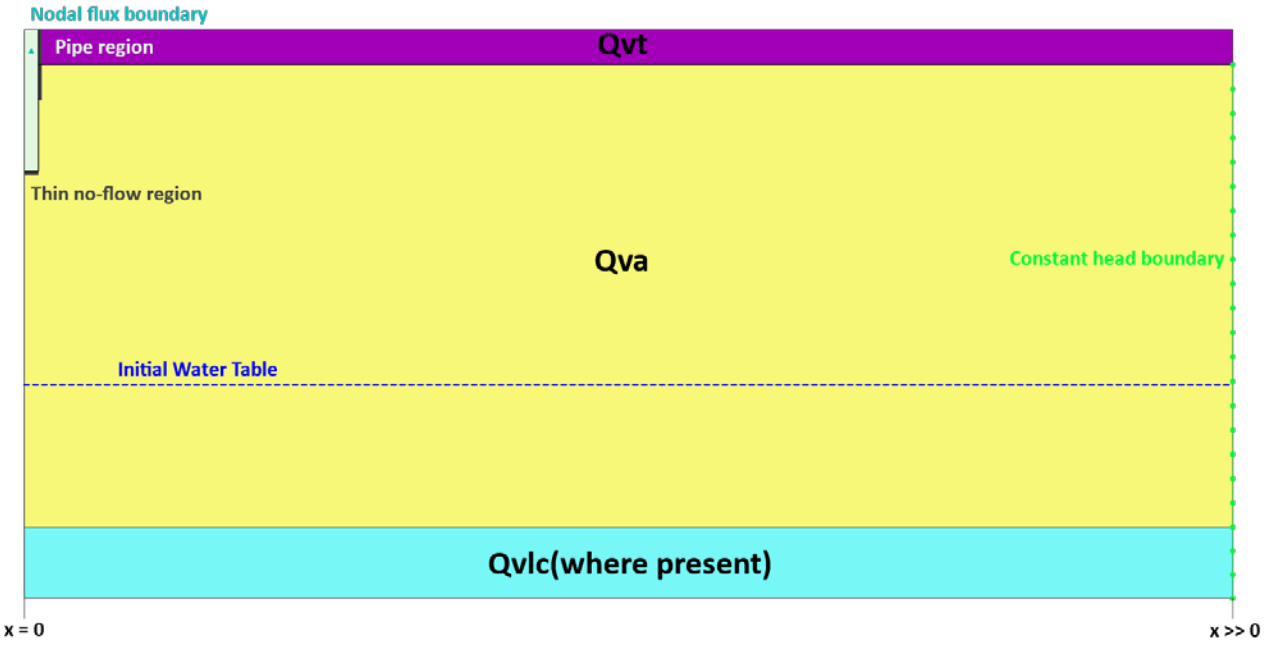

Governing Equations

SEEP/W assumes Darcy's Law applies to both saturated and unsaturated subsurface flow. SEEP/W computes the Darcy velocity, which is the product of the linear velocity and the effective porosity of the soil, or in the case of unsaturated flow the volumetric water content (θ). The matric suction and

volumetric water content ($\Psi - \theta$) relationship, commonly known as the Soil Water Retention Curve (WRC) or Soil Water Characteristic Curve (SWCC), is known as the Volumetric Water Content curve (VWC) in SEEP/W. The SWCC or WRC defines the percent saturation in the vadose zone at a given negative Ψ, which is material-specific. To further complicate things, the curve is different depending on the history of the soil, whether wetting or drying, an effect known as hysteresis. Mathematical estimation methods typically estimate the drying curve. Laboratory methods, such as the capillary-rise tests, measure the wetting process. The VWC is different that the SWCC or WRC in that it relates the pore-water pressure (u_w), rather than Ψ, to θ.

In a transient model with an applied boundary flux, the general differential equation for two-dimensional gravity-driven flow is:

$$\frac{\partial}{\partial h}\left(K_h \frac{\partial H}{\partial h}\right) + \frac{\partial}{\partial v}\left(K_v \frac{\partial H}{\partial v}\right) + Q = \frac{\partial \theta}{\partial t}$$

Which can be simplified from Bernoulli's equation:

$$H = \frac{u_w}{\gamma_w} + y$$

And the slope of the volumetric water content curve:

$$\partial\theta = m_w \partial u_w$$

To obtain:

$$\partial\theta = m_w \gamma_w \partial(H - y)$$

Figure 3: The volumetric water content curve in SEEP/W uses pore-water pressure (u_w) instead of Ψ. From GEO-SLOPE International (2012)

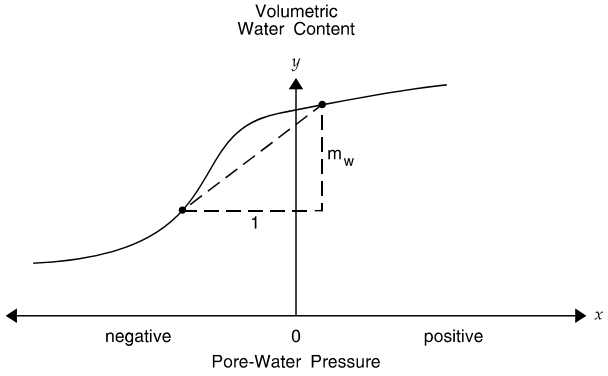

Which is substituted into the following storage equation used in SEEP/W finite element analysis:

$$\frac{\partial}{\partial h}\left(K_h \frac{\partial H}{\partial h}\right) + \frac{\partial}{\partial v}\left(K_v \frac{\partial H}{\partial v}\right) + Q = m_w \gamma_w \frac{\partial H}{\partial t} \qquad \text{(Eq. 5)}$$

Since the node elevation is constant, the elevation head term is removed. The resulting total heads that are computed from equation 5 are dependent upon the K_{sat}, the K_h:K_v, and how the VWC function is defined. As shown in Figure 3, the storage term m_w is the slope of the VWC from any neighboring time-steps.

Material Properties

Accurate numerical models for unsaturated and variably saturated flow require knowledge on both unsaturated and saturated material properties. These properties include the K_{sat} and the VWC, which are used to define the unsaturated hydraulic conductivity curve. A few options are available in SEEP/W to estimate the VWC. The software includes sample VWC functions for basic soil textures, such as sand or gravel, but these have no source information and cannot be altered. Another option is the Modified Kovacs (MK) method which estimates the VWC function using a few geotechnical properties: the

Coefficient of Uniformity (i.e. D_{60} and D_{10}) and Liquid Limit (Kovács, 1981; Aubertin et al., 2003). The VWC can be more accurately determined across the entire range of pressure heads by the closed-form solutions from Van Genuchten (1980) or Fredlund and Xing (1994), but these require fitting parameters that are determined from laboratory tests. A study by Godt and McKenna (2008) provides values for the Van Genuchten fitting parameters but their capillary rise tests are performed on Q_{va} that is disturbed (colluvium), not in-place. Inherently, their observed porosity of 0.51 is more than twice the value of 0.22 assumed in this study. The single Godt and McKenna (2008) VWC may not accurately represent the hydrogeologic properties of in-situ Q_{va}, specifically its glacial over-consolidation, structure, and grain-size distribution.

Figure 4: Volumetric water content functions considered in this study. Curves that are hysteretic are labeled in the legend.

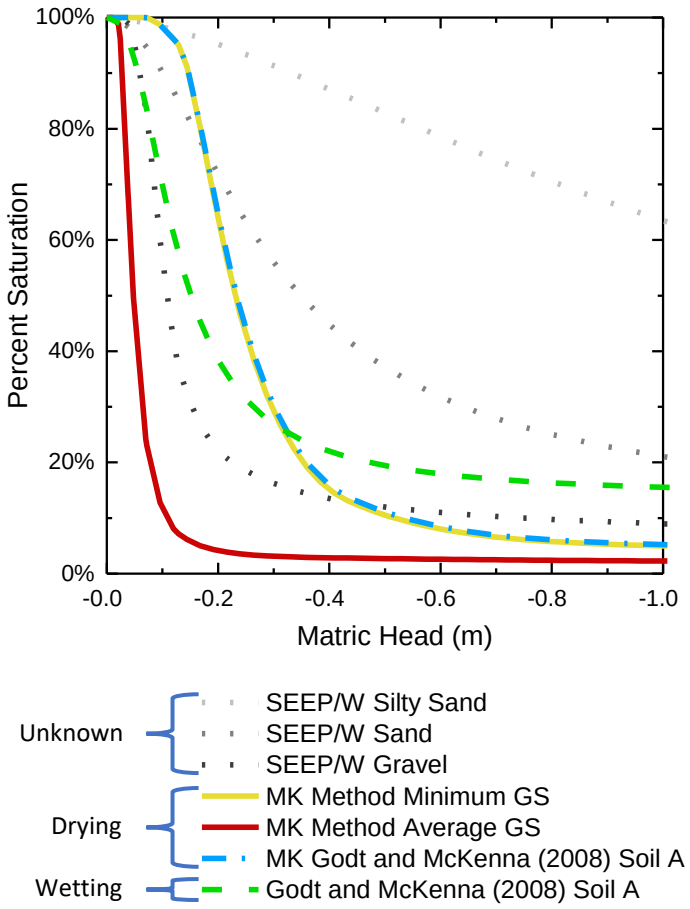

The most appropriate method to capture variations in site conditions is the MK method because AESI does multiple sieve analyses per UIC well. It should be noted that SEEP/W does not allow the fitting parameters in the MK method, which adjust the curve based on soil texture, to be changed by the user. Depending on the liquid limit, the curve is generalized into plastic-cohesive or granular soils with fitting parameter values of $m = 3 \times 10^{-5}$ and $a = 7 \times 10^{-4}$, and $m = 1$ and $a = 0.01$, respectively. The divide between these two occurs at 30% liquid limit. A comparison of the SEEP/W sample VWCs, MK method calculated curves, and the Godt and McKenna (2008) measured curves is shown in Figure 4.

The software provides two methods that translate the VWC into the unsaturated hydraulic conductivity function. The Fredlund et al. (1994) unsaturated hydraulic conductivity function method is chosen over the Van Genuchten (1980) method for two reasons: it does not rely on the residual water content parameter and it accounts for thin film or adsorptive dominated flow in the increasingly negative values of matric suction. Theoretical and experimental findings show that thin film (adsorptive) flow dominates over capillary flow in dry porous media (Lebeau and Konrad, 2010). The hydraulic conductivity estimation method of Fredlund et al. (1994) shares a similar shape to that proposed by Lebeau and Konrad (2010). The result is higher values of hydraulic conductivity in drier soil conditions (Figure 5).

The material models are comprised of three key components: the Q_{va}, the casing, and the inner-pipe region. The Q_{va} uses an unsaturated-saturated material model using the conductivity and VWC functions defined above. Using the interface material model with a tangential and normal conductivity of zero, a

Figure 5: (A) Comparison of two unsaturated K functions in SEEP/W. (B) figure from Lebeau and Konrad (2010) showing components of capillary and adsorptive flow

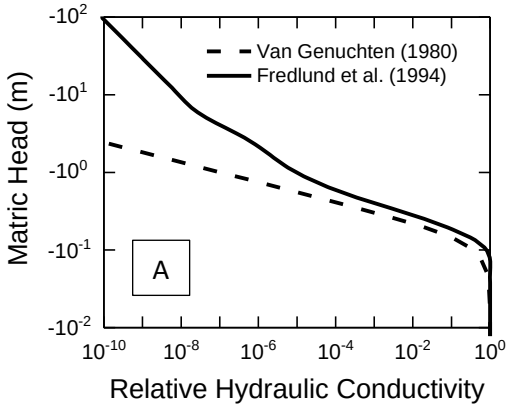

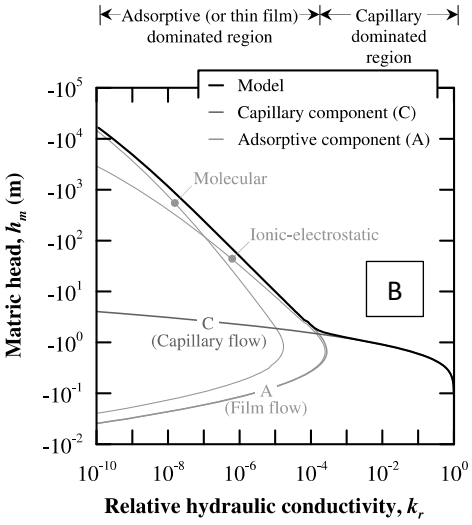

thin impermeable model is applied along the boundary of the well (i.e. casing) to direct flow through the screened interval. Finally, to allow nodal source boundary conditions to be applied inside the UIC well, an appropriate unsaturated-saturated model must be defined for this region. I assume the maximum flow under gravity using the Manning's equation with n = 0.01 for each pipe diameter. The flow velocity for completely full pipes is in the range of 100,000+ feet per hour, thus the conductivity of all pipes in the model will be defined as a constant value of 90,000 feet per hour across all pore-water pressures. Values greater than 10,000 feet per hour show no visual change in the model. While the Q_{vt} is also present in the model, it does not receive infiltration from the UIC wells and will not be discussed further. The material models are applied as shown in Figure 6. Both the unsaturated-saturated and saturated material models allow for the anisotropy of conductivity to be applied. In SEEP/W, the conductivity ratio is defined as $K_{ratio} = K_v / K_h$. I use values of 1 and 0.1 in the Q_{va} for conductivity ratios of 1:1 and 10:1 mentioned in this report.

Figure 6: Different boundary conditions as applied in each model type - (Left) Defining Head (Right) Defining Flux

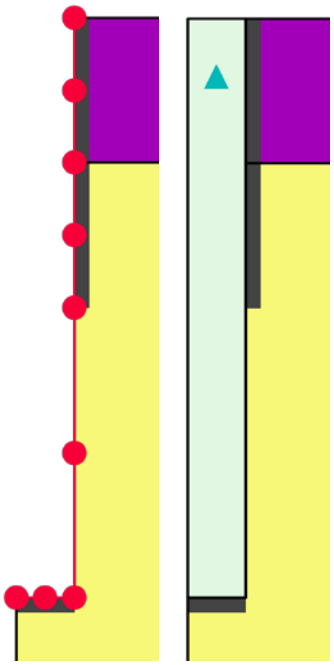

Borehole Boundary Conditions

SEEP/W allows the user to specify constant boundary conditions and functions to control head (H) or nodal flux (Q) with time. The head vs time function can be defined from reduced water-level logger data and the spline curve fit. The head boundary condition is applied along the perimeter of the well (Figure 6). The nodal flux vs. time function can be defined from flowmeter discharge readings and the step function. The flux boundary condition is applied at a point near the top of the well as a source of water into the model (Figure 6).

Meshing

Defining a suitable mesh helps in reducing un-converged nodes, decreasing runtime, and producing more definite results. In GeoStudio, meshing can be defined globally, within regions, and along lines or points. I defined the global mesh at 10 feet and a smaller 2-foot mesh inside of the well, along the perimeter of the

well with using interface elements, and along lines or points beneath the well that extend to the water table with a minimum 100-foot radius. Higher densities of nodes exclusive to these areas creates a smoother profile of the groundwater mound and bulb of saturation surrounding the well while minimizing the impact on model runtime. The interface elements on the perimeter of the well should not exceed the radius of the well, otherwise meshing errors occur. All models use the default mesh pattern of quadrangles and triangles.

METHODS

Calibration and Radius of Influence

For stepped-rate infiltration tests, constant flux and constant head are calibrated to their corresponding observed head or flux. At each site, the borehole geometry, VWC from MK method, and the depth to water table are changed. When defining head, K_{model} is changed to match the total volume flux from an 8-hour test run at the observed flow rate within ±1.0% at K_h:K_v = 1:1 and 10:1. When defining flux, K_{model} is changed until the maximum computed head matches the maximum observed head during an 8-hour test within ±1.0% at both K_h:K_v = 1:1 and 10:1. These methods are different in their approach because the former does not have hydraulic head building up during the test because a constant head is defined immediately after initial conditions, whereas the latter does have hydraulic head building up through the model and thus the maximum computed head at the end of the transient analysis is used. An 8-hour period was sufficient for the head rise to reach a near steady-state condition in the flux-defined models. Inputting flux is preferred for both transient and steady-state analysis and is the method of comparison in the results.

Specific values for the radius of influence are not provided in this study because of its varying definitions and dependence on storage effects of the unsaturated zone. The radius of influence herein is defined as the radius of the bulb of saturation surrounding the well, and the length of mound measured where the mound decays 90% from the maximum amplitude in the x-direction from the well. Other commonly used definitions are where the mounding height becomes less than one foot or less than one-quarter foot. The amount of available storage above the aquifer is dependent on the distance from the aquifer, soil heterogeneity, the effective porosity, and initial soil-moisture conditions. Unsaturated flow analysis by Sumner et al. (1999) shows that groundwater mounding decreased with increasing distance to the aquifer. In effect, an increase in storage amplifies the mediating aspects of the unsaturated zone, most prominently in transient events such as borehole infiltration tests and becoming negligible approaching steady-state conditions (Sumner et al., 1999). The behavior of the groundwater mound is therefore assessed in a qualitative manner in the sensitivity analysis.

Borehole Permeameter Solutions and Capillarity

Model results are compared to 6 different BP solutions: the original analytical Glover solution from Zangar (1953), the half-source solution in Reynolds (1983), two regressions from Stephen's (1979, 1987) based on numerical simulations, the empirical curve fit to Reynolds (1986) by Zhang (1998), and the Reynolds (2010) solution which shares the form of the Glover solution. An overview of these solutions is presented in Table 1.

Following the study by Weitering (2015), a sorptive parameter value of 5 m^{-1} is first assumed for solutions by Stephens (1979, 1987) and Reynolds (2010). Then, the sorptive parameter is fitted to match K_{model} in Microsoft Excel. The Excel solver objective is set to minimize the Root Mean Square Error

(RMSE) between $K_{analytical}$ and the K_{model} by adjusting the α-value in the shape factor (Stephens 1979, 1987) or conductivity equation (Reynolds 2010). Typically, the RMSE is used to evaluate the difference between model-predicted values and observed values. In this case, the SEEP/W is a physically-based model that is calibrated to match observed water level or flow rate, and the analytical BP methods are predictive solutions that are designed to be obtained solely through a few parameters. Lastly, to investigate the significance of the sorptive parameter, α-values are back-calculated for each step test using Excel solver by setting the objective of $K_{analytical}$ equal to their respective K_{model}.

BP solutions are evaluated on their predictive strength using the mean error (ME), mean absolute error (MAE), and the normalized root mean square error (NRMSE). The NRMSE is calculated from the difference between the model-calibrated saturated conductivity and the BP-predicted saturated conductivity. The NRMSE is the square root of the average of squared errors (RMSE) divided by the range of model values; normalization enables comparison between separate datasets. In this instance, the equation for NRMSE is

$$NRMSE = \frac{\sqrt{\frac{\sum_{i=1}^{n}\left(K_{analytical} - K_{model}\right)^2}{n}}}{K_{model_{max}} - K_{model_{min}}}$$

Table 1: Overview of borehole permeameter solution inputs and equations

Borehole Permeameter Solution	Year	Inputs				Shape Factor Equation	K_{sat} Equation
		H	r	L	α		
Glover	1953	✓	✓			$C = \sinh^{-1}\left(\frac{H}{r}\right) - \sqrt{\left(\frac{r}{H}\right)^2 + 1} + \frac{r}{H}$	K_1
Stephens	1979	✓	✓		✓	$C = 10^{\left(-0.658\log\left(\frac{H}{r}\right)+0.238\sqrt{\alpha}-0.398\log(H)+1.342\right)}$	K_2
Reynolds	1983	✓	✓			$C = 4\left[\frac{1}{2}\sinh^{-1}\left(\frac{H}{2r}\right) - \sqrt{\left(\frac{r}{H}\right)^2 + \frac{1}{4}} + \frac{r}{H}\right]$	K_1
Stephens	1987	✓	✓		✓	$C = 10^{\left(-0.486\log\left(\frac{H}{r}\right)+0.4(\alpha)-0.454\log(H)+0.019\sqrt{\frac{H}{r}}+0.828\right)}$	K_2
Zhang	1998	✓	✓			$C = \left[\frac{\frac{H}{r}}{2.074 + 0.093\left(\frac{H}{r}\right)}\right]^{0.754}$	K_1
Reynolds	2010		✓	✓		$C = \sinh^{-1}\left(\frac{L}{r}\right) - \sqrt{\left(\frac{r}{L}\right)^2 + 1} + \frac{r}{L}$	K_3

Sensitivity Analysis

The response to K_{model} and radius of influence is investigated through increasing or decreasing inputs for material properties such as the hydraulic conductivity ratio, saturated water content, and the shape of the VWC curve. The control model shares similar geometry and inputs to several UIC wells considered in this study. The base case model uses the sample VWC curve for sand with a porosity of 0.25, a saturated conductivity of 40 feet per day with a vertical anisotropy of 10:1, and an input flux of 125 gallons per minute. The control borehole has a radius of 1/3 foot, a screen length of 25.5 feet, and a 50 foot depth to water table. First, the vertical anisotropy is changed to 1:1 and 100:1. Next, the saturated water content (porosity) is changed to 0.15 and 0.35. Finally, the shape of the volumetric water content curve is changed to SEEP/W sample functions for gravel and silty sand. Each version is run for 20 days and the isolines where $u_w = 0$ are plotted after 1, 3, 5, and 20 days.

RESULTS

Calibration

All constant head and flux steps were successfully calibrated to ±1% difference in observed flux or head. Minor differences in K_{model} between the head and flux-based models are listed in Appendix A: Model and Analytical Results. Eleven UIC well infiltration tests have multiple steps that reached quasi-steady state conditions and nine of these tests have steps that are associated with different percentages of the screen. As the Q_{va} sometimes coarsens upward, the majority of the nine steps follow the expectation of higher K_{model} at higher steps (Figure 7). The change in these select tests from K_{model} at the lower step to K_{model} at the higher step ranges from -21% to +70% for isotropic and -31% to +57% for anisotropic medium.

Figure 7: Change in K from lower to higher head tests when the higher head test involved a larger portion of the screen [L].

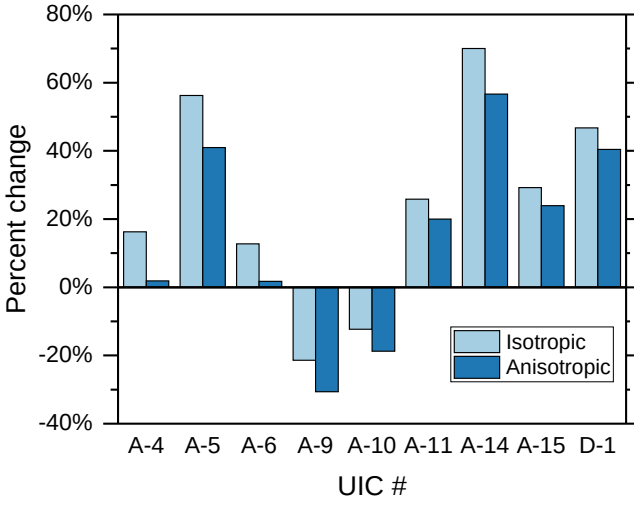

Comparison with BP methods

When assuming an α-value of 5 m^{-1}, the order of models (where H < L) that calculate $K_{analytical}$ from lowest to highest are Glover, Zhang, Reynolds (1983), then Stephens (1979) and Stephens (1987). Figure 8 show graphs comparing SEEP/W K_{model} to $K_{analytical}$ from select BP solutions at isotropic and a vertical anisotropy of 10:1. The solutions that best match model results plot along the x=y line. The solutions that have the lowest error values are the Reynolds (2010) and Zhang (1998) equation (Table 2). Both the Stephens equations had large errors with the assumed sorptive number value of 5m^{-1}. While the solutions were intended for isotropic media, I assess their predictions at the vertical anisotropy of 10:1 that is typical for the Q_{va}. At this conductivity ratio, the solution by Reynolds (1983) gives results with low errors (Table 3).

Figure 8: (above) Graph comparing K (feet/day) calculated in SEEP/W to BP methods at K_h:K_v = 1:1 and sorptive numbers specified in Table 2. (below) Graph comparing K (feet/day) calculated in SEEP/W to BP methods at K_h:K_v = 10:1 and sorptive numbers as specified in Table 2

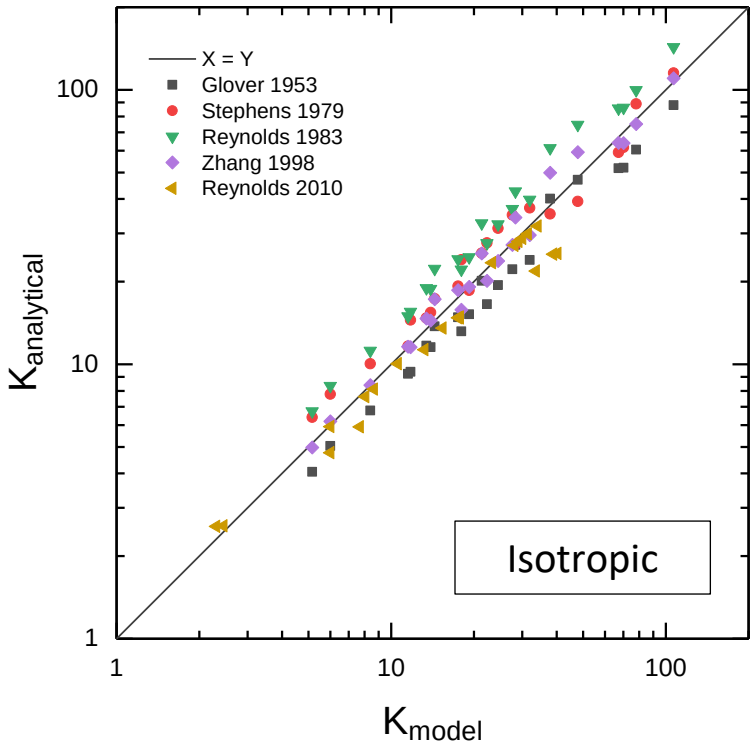

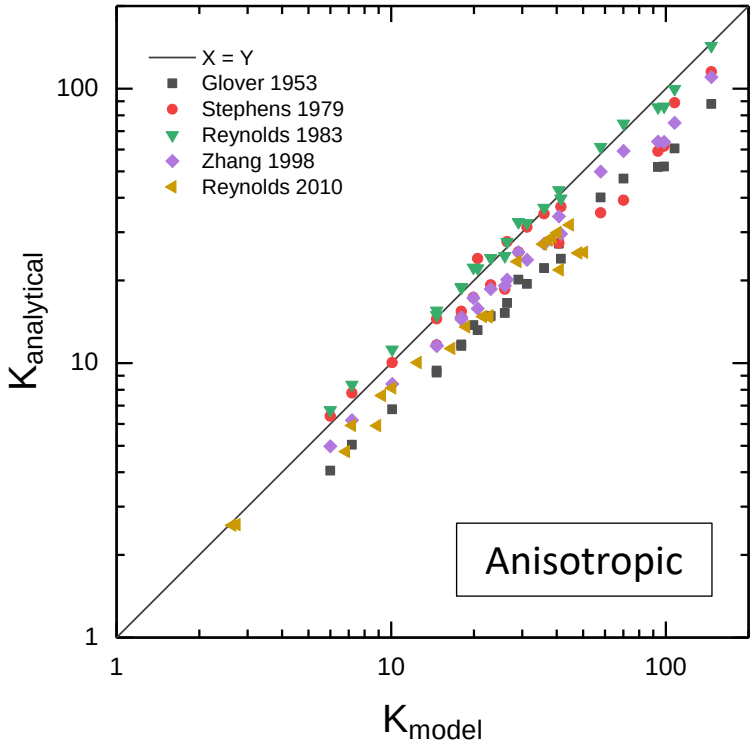

Table 2: Summary of ME, MAE, and RMSE for $K_{analytical}$ relative to isotropic K_{model}. [1]$\alpha=5m^{-1}$, [2]$\alpha=2.1m^{-1}$, [3]$\alpha=1.1m^{-1}$

BP Solution	Error		
	ME	MAE	RMSE
Glover 1953	-16%	17%	8%
Reynolds 1983	36%	36%	13%
Stephens 1979[1]	65%	65%	21%
Stephens 1987[1]	107%	107%	36%
Stephens 1979[2]	7%	14%	5%
Stephens 1987[3]	7%	16%	6%
Zhang 1998	4%	9%	4%
Reynolds 2010[1]	-13%	14%	5%

Table 3: ME, MAE, and RMSE for Reynolds (1983) $K_{analytical}$ to anisotropic K_{model}

BP Solution	Error		
	ME	MAE	RMSE
Reynolds 1983	4%	7%	4%

Table 4: RMSE fitted sorptive number values from Stephen's (1979, 1987) and Reynolds (2010) solutions in comparison to value assumed in Weitering (2015)

Equation	α (m^{-1})	α (ft^{-1})
Stephens (1979) in Weitering (2015)	4.6	15
Stephens-I (1979)	2.1	0.6
Stephens-II (1987)	1.1	0.3
Reynolds (2010)	∞	∞

Figure 9: Stephens (1979) equation sorptive numbers fitted each step individually to match isotropic K_{model}. Sorptive numbers decrease exponentially with head rise in tests where the head [H] is less than the length of the screen [L].

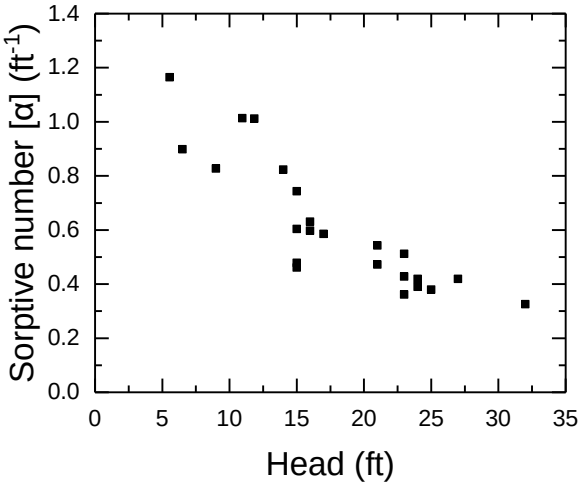

Table 5: Capillarity descriptions modified from Reynolds and Elrick (1985)

Soil texture and structure	Capillarity	α (ft^{-1})
Compacted, Structure-less, clayey or silty materials such as lacustrine or marine sediments.	very high	0.3
Soils which are both fine textured (clayey or silty) and unstructured; may also include some fine sands.	high	1.2
Most structured soils from clays through loams; also includes unstructured medium and fine sands.	moderate	3.7
Coarse and gravely sands; may also include some highly structured soils.	low	11
Gravels and very coarse sands containing negligible amounts of fine-grained material	negligible	∞

Fitted sorptive numbers (α) are not comparable between solutions. The fitted α-values in Stephen's fall below expected values based on previous work by Weitering (2015). In that study, a reasonable number of ~$5m^{-1}$ was assumed for the Q_{va} based on an alternative equation in Stephens (1979). The fitted α-values are lower in this study than used by Weitering (Table 4) and suggest the Q_{va} has a high to very high capillarity. According to Table 5, this range of sorptive numbers is most consistent with finely textured (fine sand) to predominantly clayey or silty material. If the values for each test are fitted individually, α values decrease exponentially with increasing head (Figure 9). Fitted sorptive numbers in Reynolds (2010) approach infinity and are approximated as such. Infinite sorptive numbers are associated with negligable capillarity, which is assumed in gravels and very coarse sands.

Sensitivity Analysis

Model calibration and the radius of influence are more sensitive to some variables than others. Increasing the vertical anisotropy decreases mound height and increases the radius of influence. Isotropic soil has the smallest radius and longest vertical extension of the bulb of saturation surrounding the well. When changing from isotropic to anisotropic the results show an average ~30% increase in K_{model}. An increase in lateral flow is required to reproduce identical conditions in the UIC well under limited vertical flow. Increasing the saturated water content from 0.15 to 0.35 results in an insignificant change in the calibrated conductivity and does not affect the steady-state condition in the model, only the time is taken to reach that state (Figure 11). Lower porosities reduce the time required to reach the steady-state condition of the mound. Shifting the volumetric water content function from silty sand to gravel slightly impacted the amplitude and radial extent of the groundwater mound, with silty sand causing the largest mound. Altering the water content curve to silt or finer materials caused the model to have difficulty converging, these curves could not be considered in the sensitivity analysis. Between the three material properties considered above, the anisotropy of the Q_{va} hydraulic conductivity is most impactful to model calibration and the radius of influence of UIC Well infiltration.

Some model assumptions may have a significant or insignificant effect on the result calculated in the model. One major assumption in the model is that borehole development has no influence in the results, however, in one case where a UIC well was re-developed to address known issues and increase performance, the modeled saturated conductivity increased by more than 100%. Conversely, the accuracy of flowmeters (±2%) (State of Washington Department of Ecology - Water Resources, 2017) has a low effect on the results.

Figure 10: Base case or control model for the sensitivity analysis. The bottom of the well is at 200 feet and the initial water table begins at 150 feet elevation. Isolines for the initial water table and after 1, 3, 5, and 20 days are marked.

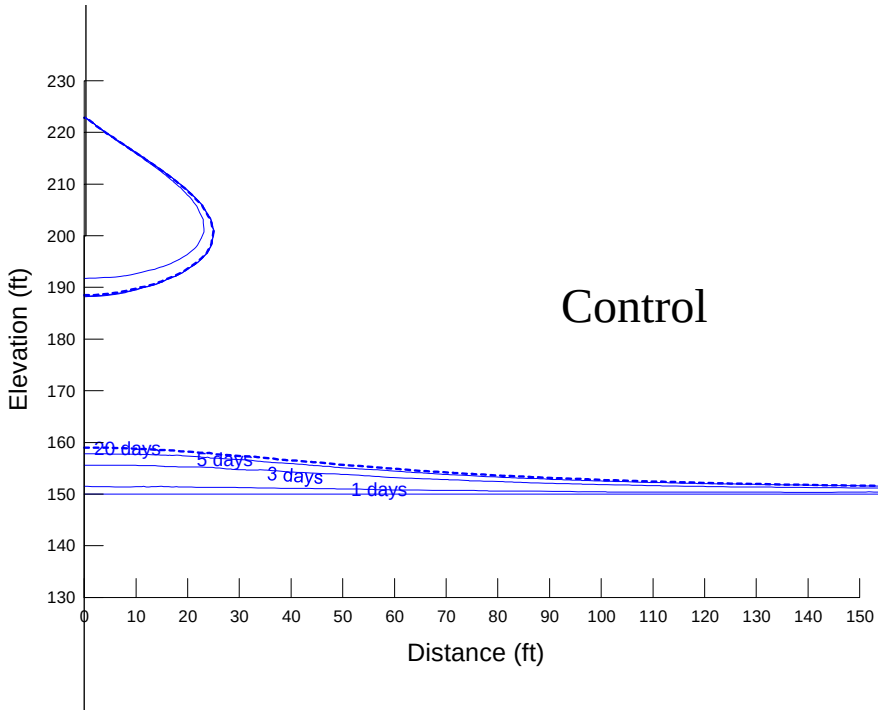

Figure 11: Results of the sensitivity analysis: (A) Porosity decreased to 0.15; (B) porosity increased to 0.35; (C) VWC curve changed to silty sand; (D) VWC curve changed to gravel; (E) Isotropic medium; (F) Anisotropy increased to 100:1.

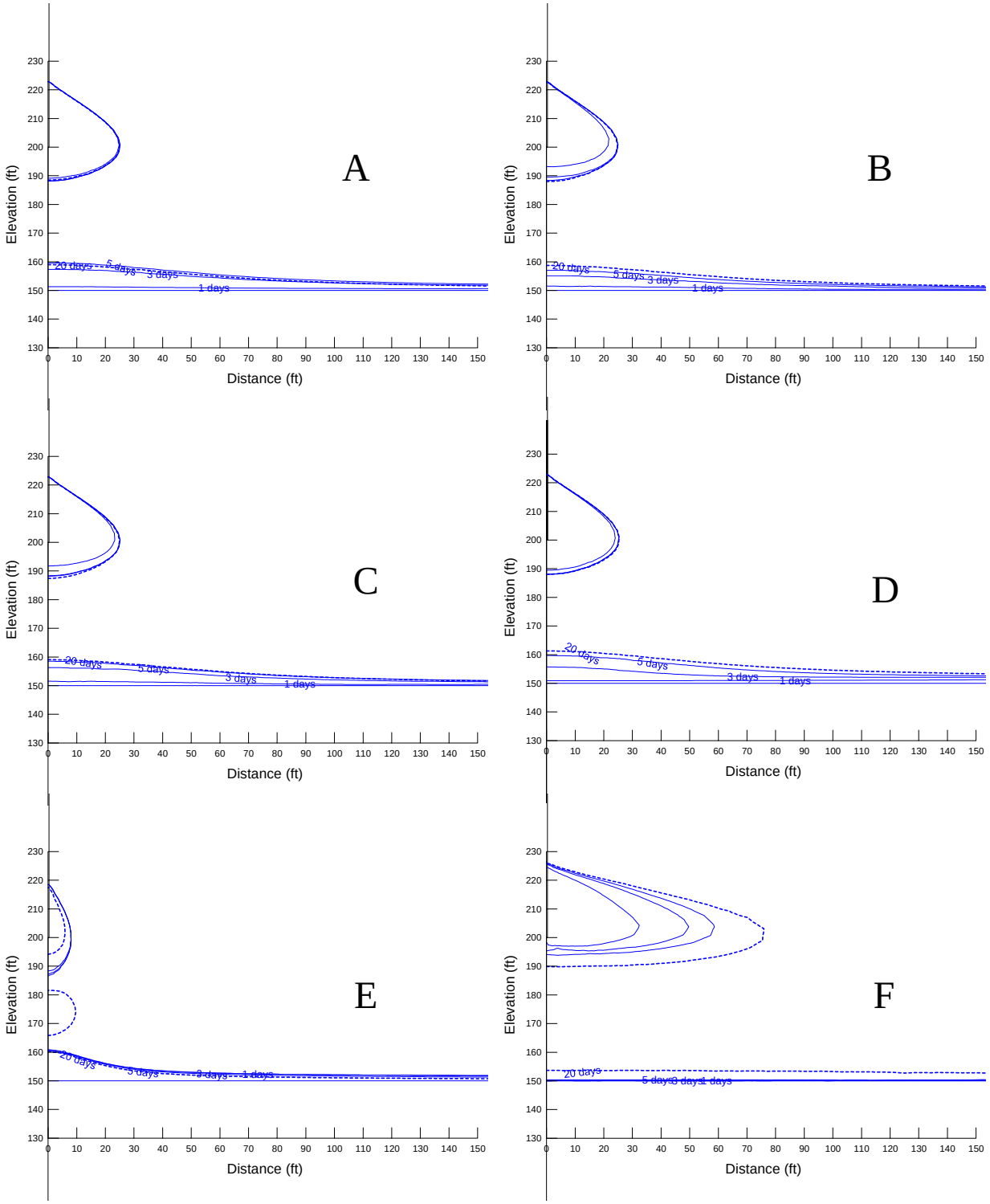

DISCUSSION AND CONCLUSIONS

Future Groundwater Mounding Analyses

All models must make assumptions based on unknown parameters or to simplify real-world processes for efficiency and budgetary reasons. As shown in the results of the sensitivity analysis, the radius of influence is most affected by the definition of the anisotropy. Common software methods (MODRET/MODFLOW) that do not account for anisotropy or unsaturated flow may insufficiently predict the height or extent of the groundwater mound from infiltration structures. MODRET, a one-layer aquifer model, does not account for vertical anisotropy while MODFLOW can only incorporate anisotropy using multiple layers (Carleton, 2010). In the USGS report by Carleton, adding multiple layers in MODFLOW increased the mound height with little change to the radius of influence in comparison to a single-layer MODFLOW. The results of this study show that under unsaturated flow, the inclusion of anisotropy decreases the mound height and increases the radius of influence relative to the isotropic model. Unsaturated finite difference analysis by Sumner et al. (1999) also concluded that the addition of vertical anisotropy or a fine-textured layer significantly decreases the mounding height in comparison to the base isotropic model. Future studies that evaluate groundwater mounding beneath infiltration facilities should incorporate the effects of unsaturated flow and reasonable values for anisotropy based on either field tests or a hydrogeologic conceptual model.

Borehole Permeameter Solutions and the Sorptive Number

On the other hand, BP solutions make numerous assumptions and produce values of saturated conductivity within fraction of an order of magnitude than calibrated in SEEP/W in this study. Zhang's (1998) solution for sand is a simple equation for $K_{analytical}$ with 9% mean absolute error (MAE) and can be used when the head is less than the screen length. A less simple equation from Reynolds (2010) accounts for the screen length with $K_{analytical}$ values of 13% MAE. Under 10:1 vertical anisotropy the $K_{analytical}$ values from Reynolds (1983) have 7% MAE.

Following the suggestion by Weitering (2015) to further investigate the capillarity parameter or sorptive number (α), I have found that it is more sensitive in Stephens (1979, 1987) regressions than in solutions that share the form of equation 1, such as Reynolds (2010). First, the expected texture and structure based on fitted Stephens values are vastly different opposed to fitted Reynolds values. Fitted values from both Stephens solutions relate to texture that is much finer than the Q_{va}, whereas fitted Reynolds values approach infinity and suggest the Q_{va} has negligable capillarity. Capillary is assumed to be negligable in coarse sand and gravel, which is nearly the Q_{va} grain size observed across most of the sites considered in this study (see Appendix B: Borehole Geometry, Infiltration Test Summary, and Grain Size). Secondly, the sorptive number in Stephens equations decreasingly trends with increasing head levels, suggesting that the sorptive number acts more like a fitting parameter than a number with clear physical significance. All in all, the sorptive number is highly dependent on the overall fit of the analytical solution in which it is applied.

This study finds that the best solutions predict K_{sat} with a roughly 10% MAE without the use of the sorptive number, and these equations can be readily applied to the results of a borehole infiltration test to estimate average K_{sat} of the material within the screened portion of the well. This study also distinguishes that the BP solution by Reynolds (1983) can be applied to anisotropic material with more accurate estimations than other BP solutions. Freeze and Cherry state that vertical anisotropy in cores rarely exceeds 10:1, but the cumulative effect of multiple less permeable layers could lead to a vertical anisotropy of 10:1 or greater (Freeze and Cherry, 1979). A combination of the Zhang (1998) or Reynolds

(2010) and the Reynolds (1983) solutions can be used to estimate K_{sat} at vertical anisotropy between 10:1 and isotropic media.

Impact on Regional Regulations and Design

The Washington State Department of Ecology's 2006 manual titled *Guidance for UIC Wells that Manage Stormwater* gives specific information for UIC well design such as siting advisements and vadose zone treatment capacity requirements. In the section concerning vadose zone treatment capacity, the manual states that significant mounding can occur from UIC well discharge and the well must not discharge stormwater directly into the rising groundwater mound. In addition, the medium-rated water quality treatment capacity of the Q_{va} requires a 10-foot thick zone of unsaturated flow to be maintained. The height of the groundwater mound and the size of the bulb of saturation from UIC well infiltration is strongly sensitive to the vertical anisotropy. Isotropic soil has the highest mounding and longest vertical extension of the bulb of saturation, the combination of these two observations is that isotropic soils with shallow water tables are more prone to failing protective requirements set by the manual.

The radius of influence is most influential to off-site impacts and in transient models the radius changes with time. As modeled, these stepped-rate infiltration tests reflect a pulse of water in the subsurface that arrives at the water table within the same period. The peak amplitude occurs as most of the wetting front reaches the water table. Thereafter the mound diffuses, increasing the radius of influence with decreasing effect. Thus, radius of influence as defined in this study captures the maximum effect of the mound at the smallest radius of influence. Although the infiltration tests are designed to stress the system beyond design flow rates, they are transient. The radius of influence from infiltration tests should be treated as a minimum value; more conservative numbers can be and are obtained from hydrographs or constant flow rates over longer periods, like that presented in the sensitivity analysis.

The Washington State Department of Ecology's manual (2006) does not require, and this study does not provide specific numbers relating to UIC well spacing or setback from slopes. A more rigorous analysis of groundwater mounding including regional flow directions and site-specific conditions would typically be performed by a licensed consultant and this report can be used as an aid in the modeling process and sensitivity specific to these structures.

REFERENCES

Armstrong, J.E., Crandell, D.R., Easterbrook, D.J., and Noble, J.B., 1965, Late pleistocene stratigraphy and chronology in southwestern British Columbia and northwestern Washington: Bulletin of the Geological Society of America, v. LXXVI, p. 321–330, doi: 10.1130/0016-7606(1965)76[321:LPSACI]2.0.CO;2.

Aubertin, M., Mbonimpa, M., Bussière, B., and Chapuis, R.P., 2003, A model to predict the water retention curve from basic geotechnical properties: Canadian Geotechnical Journal, v. XL, p. 1104–1122, doi: 10.1139/t03-054.

Booth, D.B., and Hallet, B., 1993, Channel networks carved by subglacial water—observations and reconstruction in the eastern Puget Lowland of Washington: Geological Society of America Bulletin, v. 105, p. 671–683.

Carleton, G.B., 2010, Simulation of Groundwater Mounding Beneath Hypothetical Stormwater Infiltration Basins: U.S. Geological Survey, https://pubs.usgs.gov/sir/2010/5102/support/sir2010-5102.pdf.

Chapuis, R.P., 1998, Overdamped slug test in monitoring wells: Review of interpretation methods with mathematical, physical, and numerical analysis of storativity influence: Canadian Geotechnical Journal, v. XXXV, p. 697–719, doi: 10.1139/t98-041.

DHI Water and Environment, 2009, Vashon-Maury Island Hydrologic Modeling: https://your.kingcounty.gov/dnrp/library/2009/kcr2080.pdf.

Elrick, D.E., Reynolds, W.D., and Tan, K.A., 1989, Hydraulic Conductivity Measurements in the Unsaturated Zone Using Improved Well Analyses: Grounwater Monitoring And Remediation, v. IX, p. 184–193.

Fetter, C.W., 2001, Applied Hydrogeology (P. Lynch, Ed.): Upper Saddle River, New Jearsey USA, Prentice-Hall Inc., 615 p.

Fredlund, D.G., Xing, A., and Huang, S., 1994, Predicting the permeability function for unsaturated soils using the soil-water characteristic curve: Canadian Geotechnical Journal, v. 31, p. 533–546, doi: 10.1139/t94-062.

Freeze, R., and Cherry, J.A., 1979, Groundwater: Englewood Cliffs, New Jearsey USA, Prentice-Hall Inc., 604 p.

Galster, R., and Laprade, W., 1991, Geology of Seattle, Washington, United States of America: Environmental & Engineering Geoscience, v. XXVIII, p. 235–302.

GEO-SLOPE International, 2012, Seepage Modeling with SEEP/W: Geostudio Helpfile, p. 207, http://downloads.geo-slope.com/geostudioresources/8/0/6/books/seep modeling.pdf?v=8.0.7.6129.

Joint Institute for the Study of the Atmosphere and Ocean, 2009, Puget Sound Lowland Precipitation and Surface Temperature 1895 - January 2009: http://research.jisao.washington.edu/data_sets/climate_division/puget_sound.html.

Kovács, G., 1981, Seepage Hydraulics: Amsterdam, Netherlands, Elsevier Science Publishers, 730 p.

Lebeau, M., and Konrad, J.-M., 2010, A new capillary and thin film flow model for predicting the hydraulic conductivity of unsaturated porous media: Water Resources Research, v. 46, p. 1–15, doi: 10.1029/2010WR009092.

Morgan, D.S., and Jones, J.L., 1996, Numerical model analysis of the effects of ground-water withdrawals on discharge to streams and springs in small basins typical of the Puget Sound lowland, Washington: 1-73 p., http://cat.inist.fr/?aModele=afficheN&cpsidt=13720588.

Porter, S.C., and Swanson, T.W., 1998, Radiocarbon Age Constraints on Rates of Advance and Retreat of the Puget Lobe of the Cordilleran Ice Sheet during the Last Glaciation: Quaternary Research, v. 50, p. 205–213, doi: 10.1006/qres.1998.2004.

Reynolds, W.D., 2010, Measuring Soil Hydraulic Properties Using a Cased Borehole Permeameter: Steady Flow Analyses: Vadose Zone Journal, v. 9, p. 637, doi: 10.2136/vzj2009.0136.

Reynolds, W.D., and Elrick, D.E., 1985, The Constant Head Well Permeameter: Effect of Unsaturated Flow.: Soil Science, v. 139, p. 172–180.

Reynolds, W.D., Elrick, D.E., and Topp, G.C., 1983, A reexamination of the constant head well permeameter method for measuring saturated hydraulic conductivity above the water table1: Soil Science, v. 136, p. 250, doi: 10.1097/00010694-198310000-00008.

State of Washington Department of Ecology - Water Resources, 2017, General Guide for the Most Common Types of Pressurized Pipe Flow Meters Used, p. 1, http://www.ecy.wa.gov/programs/wr/measuring/images/pdf/ppfm_genguide.pdf.

State of Washington Department of Ecology Water Quality Program, 2006, Guidance for UIC Wells that Manage Stormwater: State of Washington Department of Ecology, https://fortress.wa.gov/ecy/publications/documents/0510067.pdf.

Stephens, D.B., 1979, Analysis of Constant Head Borehole Infiltration Tests in the Vadose Zone: The University of Arizona, 366 p., http://hdl.handle.net/10150/191055.

Stephens, D.B., Lambert, K., and Watson, D., 1987, Regression models for hydraulic conductivity and field test of the borehole permeameter: Water Resources Research, v. XXIII, p. 2207–2214, doi: 10.1029/WR023i012p02207.

Sumner, D.M., Rolston, D.E., and Marin, M.A., 1999, Effects of Unsaturated Zone on Ground-water Mounding: Journal of Hydrologic Engineering, v. IV, p. 65–69, doi: 10.1061/(ASCE)1084-0699(1999)4:1(65).

Troost, K.G., 2016, Chronology, Lithology and Paleoenvironmental Interpretations of the Penultimate Ice-Sheet Advance into the Puget Lowland, Washington State: University of Washington, 239 p., https://digital.lib.washington.edu/researchworks/bitstream/handle/1773/38517/Troost_washington_0250E_12966.pdf?sequence=1&isAllowed=y.

Troost, K., and Booth, D., 2008, Geology of Seattle and Seattle area, Washington: Geological Society of America Reviews in Engineering Geology, p. 1–35, doi: 10.1130/2008.4020(01).

Turney, G.L., Kahle, S.C., and Dion, N.P., 1995, Geohydrology and Ground-Water Quality of East King County, Washington: U.S. Geological Survey Water-Resources Investigations Report, v. 94–4082, https://pubs.usgs.gov/wri/1994/4082/report.pdf.

U.S. Department of the Interior Bureau of Reclamation, 1990, Procedure For Constant Head Hydraulic Conductivity Tests in Single Drill Holes, *in* USBR Earth Manual Part II, v. 7310–89, p. 1245–1259, https://www.usbr.gov/tsc/techreferences/mands/mands-pdfs/earth2.pdf.

Vaccaro, J.J., Hansen, A.J., and Jones, M.A., 1998, Hydrogeologic Framework of the Puget Sound Aquifer System: U.S. Geological Survey, https://pubs.usgs.gov/pp/1424d/report.pdf.

Weitering, B., 2015, Computing Hydraulic Conductivity from Borehole Infiltration Tests and Grain-Size Distribution in Advance Glacial Outwash Deposits, Puget Lowland, Washington: University of Washington, 43 p., http://hdl.handle.net/1773/36259.

Woodward, B.D.G., Packard, F.A., Dion, N.P., and Sumioka, S.S., 1995, Occurrence and Quality of Ground Water in Southwestern King County, Washington: U.S. Geological Survey Water-Resources Investigations Report, v. 92–4098, p. 69, https://pubs.usgs.gov/wri/1992/4098/report.pdf.

Zangar, C.N., 1953, Theory And Problems Of Water Percolation: Engineering Monograph, v. VIII, p. 76, https://www.usbr.gov/tsc/techreferences/hydraulics_lab/pubs/EM/EM08.pdf.

Zhang, Z.F., Groenevelt, P.H., and Parkin, G.W., 1998, The well-shape factor for the measurement of soil hydraulic properties using the Guelph Permeameter: Soil and Tillage Research, v. 49, p. 219–221, doi: 10.1016/S0167-1987(98)00174-3.

APPENDIX A: MODEL AND ANALYTICAL RESULTS

[X] Pre-redevelopment

Test Number	Model [H] K (ft/day)		Model [Q] K (ft/day)		Analytical Methods (K in ft/day)					
	SEEP/W (1:1)	SEEP/W (10:1)	SEEP/W (1:1)	SEEP/W (10:1)	Glover 1953	Stephens 1979	Stephens 1983	Reynolds 1983	Zhang 1998	Reynolds 2010
A-1a	6.7	7.8	7.7	8.9						5.79
A-1b	7.7	9.0	8.6	10.1						8.03
A-2	4.1	4.6	5.2	6.0	4.1	6.4	6.5	6.7	5.0	
A-3a	5.9	6.7	6.0	6.8						4.66
A-3b	7.2	8.4	8.0	9.2						7.55
A-3c[X]	2.4	2.6	2.4	2.7						2.55
A-4a	16.9	21.6	19.2	25.9	15.2	18.6	18.3	24.5	19.1	
A-4b	22.6	27.1	22.3	26.4	16.5	27.7	28.3	27.6	20.1	
A-5a	11.8	14.4	11.5	14.6	9.2	11.6	11.5	15.0	11.6	
A-5b	19.3	22.1	18.0	20.6	13.2	24.0	24.6	22.2	15.8	
A-6a	31.4	43.2	28.3	40.8	27.2	27.3	25.7	42.6	34.2	
A-6b	31.2	39.8	31.9	41.5	24.0	37.1	37.7	39.8	29.5	
A-7	44.4	61.2	37.9	57.8	40.1	35.3	31.9	61.2	49.9	
A-8	12.0	14.8	11.8	14.6	9.4	14.5	14.7	15.5	11.5	
A-9a	14.5	18.7	13.4	18.0	11.7	14.7	14.6	18.9	14.7	
A-9b	10.1	11.8	10.6	12.5						9.93
A-10a	18.6	23.9	17.5	23.0	14.8	19.3	19.1	24.1	18.6	
A-10b	14.6	17.6	15.4	18.7						13.33
A-11a	13.2	16.6	13.9	18.0	11.5	15.4	15.4	18.8	14.4	
A-11b	16.6	19.4	17.5	21.6						14.52
A-12	6.4	7.6	6.0	7.2	5.0	7.8	7.9	8.3	6.2	
A-13	8.2	9.5	8.4	10.1	6.8	10.0	10.1	11.2	8.4	
A-14a	17.0	22.1	14.4	19.9	13.8	17.3	17.1	22.3	17.3	
A-14b	25.3	31.9	24.5	31.2	19.4	31.3	31.9	32.3	23.8	
A-15a	23.2	29.6	21.4	29.0	20.1	25.4	25.1	32.6	25.3	
A-15b	27.1	34.6	27.6	36.0	22.2	35.0	35.6	36.8	27.2	
A-16a	11.5	13.7	13.2	16.6						11.06
A-16b	14.4	17.3	17.8	22.8						14.62
A-16c	13.9	16.8	17.8	22.6						14.52
A-17	5.3	6.0	6.0	7.2						5.87
A-18	2.2	2.4	2.3	2.6						2.54
B-1	35.0	43.2	34.1	44.6						31.40
B-2	30.5	37.2	30.0	38.6						28.34
B-3	24.0	28.6	23.3	28.8						23.18
B-5	32.9	40.1	31.4	40.3						29.42
B-6	30.0	36.5	29.0	37.4						27.64
B-7	29.3	35.5	28.1	35.8						26.74

Test Number	Model [H] K (ft/day)		Model [Q] K (ft/day)		Analytical Methods (K in ft/day)					
	SEEP/W (1:1)	SEEP/W (10:1)	SEEP/W (1:1)	SEEP/W (10:1)	Glover 1953	Stephens 1979	Stephens 1983	Reynolds 1983	Zhang 1998	Reynolds 2010
C-1	33.4	40.3	40.3	50.4						24.99
C-2	28.6	37.2	33.6	41.0						21.57
C-3	111.1	147.4	106.8	146.4	87.9	115.2	114.6	143.1	110.1	
C-4	30.5	36.7	38.9	48.0						24.85
C-5	75.8	98.4	78.0	107.5	60.5	88.9	89.8	99.7	75.0	
D-1b	45.1	64.3	47.8	70.1	47.0	39.2	38.5	74.6	59.3	
D-1c	57.4	78.7	67.2	93.6	51.8	59.1	61.3	85.4	64.0	
D-1d	58.6	79.2	70.1	98.4	52.0	61.7	64.2	86.1	64.0	

APPENDIX B: BOREHOLE GEOMETRY, INFILTRATION TEST SUMMARY, AND GRAIN SIZE

[X] Pre-redevelopment

*No grain size data available, averaged from other UIC wells at site (if available)

Well Test ID	Borehole depth (ft)	Length of screen open to aquifer [L] (ft)	Borehole radius [r] (ft)	Depth to WT (ft)	Head [H] (ft)	Flow rate [Q] (gpm)	Averaged D_{10} (mm)	Averaged D_{60} (mm)
A-1a	66.1	25.5	0.33	161	27	33	0.17	3.76
A-1b					62	103		
A-2	93	25.5	0.33	118	24	19	1.37	7.56
A-3a	68.2	25.5	0.33	93	27	26	0.18	3.55
A-3b					64	100		
A-3c[X]					51	27		
A-4a	100	61.3	0.33	13	14	28	0.12	0.38
A-4b					27	96		
A-5a	90.2	51	0.33	10	15	19	0.13	0.71
A-5b					32	103		
A-6a	62.5	25.5	0.33	139	9	24	0.16	0.91
A-6b					23	105		
A-7	63.1	25.5	0.33	124	6.5	20	0.30	2.36
A-8	67.1	25.5	0.33	130	23	41	0.29	4.17
A-9a	61.1	25.5	0.33	116	15	24	0.43	2.71
A-9b					51	105		
A-10a	67.9	25.5	0.33	89	16	35	0.14	2.73
A-10b					38	106		
A-11a	92.9	25.5	0.33	35	17	30	0.15	1.24
A-11b					34	103		
A-12	63.9	25.5	0.33	47	23	22	0.11	0.32
A-13	64.2	25.5	0.33	8	21	25	0.11	0.32
A-14a	74.9	35.8	0.33	116	15	29	0.80	6.99
A-14b					25	98		
A-15a	67.9	25.5	0.33	102	15	42	0.15	3.20
A-15b					24	104		
A-16a	56	20	0.21	120	29	50	0.27	2.30
A-16b					36	82		
A-16c					42	95		
A-17	60	20	0.21	50	56	51	0.23	0.75
A-18	77	20	0.21	5	73	29	0.12	2.64

Well Test ID	Borehole depth (ft)	Length of screen open to aquifer [L] (ft)	Borehole radius [r] (ft)	Depth to WT (ft)	Head [H] (ft)	Flow rate [Q] (gpm)	Averaged D_{10} (mm)	Averaged D_{60} (mm)
B-1	80	30	0.25	130	41	285	0.24	0.96
B-2	80	30	0.25	130	45	282	0.24	0.79
B-3	80	30	0.25	130	52	266	0.27	1.77
B-4*	80.1	10.1	0.30	130	8	140	0.24	1.14
B-5	80	30	0.25	130	41	267	0.21	1.21
B-6	80	30	0.25	130	44	269	0.23	0.94
B-7	80	30	0.25	130	44	262	0.24	1.18
C-1	115	41	0.33	42	45	336	0.72	3.80
C-2	115	41	0.33	40	47	307	0.70	3.29
C-3	115	40	0.33	38	16	211	0.26	2.56
C-4	115	39	0.33	39	49	349	0.33	2.73
C-5	116	42	0.33	39	21	220	0.67	4.90
D-1b*	72	50	0.17	50	6	15	0.30	2.50
D-1c*					11	52		
D-1d*					12	60		